

Determining thermal dust emission from Planck HFI data using a sparse, parametric technique

Melis O. Irfan¹, Jérôme Bobin¹, and Marc-Antoine Miville-Deschénes¹

Laboratoire CosmoStat, AIM, UMR CEA-CNRS-Paris 7 Irfu, DAp/DEDIP, CEA Saclay, F-91191 GIF-SUR-YVETTE CEDEX, France.
 e-mail: melis.irfan@cea.fr

Received XXX XX, XXXX; accepted XXX XX, XXXX

ABSTRACT

Context. The *Planck* 2015 data release provided the community with high frequency ($\nu > 100$ GHz) observations of the full-sky at unprecedented resolutions. These maps contain a wealth of information on the cosmic microwave background (CMB), cosmic infrared background (CIB), extragalactic point sources and diffuse thermal dust emission.

Aims. We aim to determine the modified black body (MBB) model parameters of thermal dust emission and produce all sky maps of pure thermal dust, having separated this Galactic component from the CMB and CIB.

Methods. This separation is completed using a new, sparsity-based, parametric method which we refer to as *premise*. The method comprises of three main stages: 1) filtering of the raw data to reduce the effect of the CIB on the MBB fit. 2) fitting an MBB model to the filtered data across super-pixels of various sizes determined by the algorithm itself and 3) refining these super-pixel estimates into full resolution maps of the MBB parameters.

Results. We show

Conclusions. We believe...

Key words. Cosmology: Cosmic Microwave Background – ISM: dust, extinction – Methods: Data Analysis

0.1. Radiance maps from the MBB parameters

([Planck Collaboration et al. 2014](#)) have shown that thermal dust radiance, the integrated flux density over frequency, provides a cleaner way to view thermal dust estimates. This is because the CIBA decorrelate over frequency, leaving less of a residual impact in the radiance maps than within the optical depth estimates. We calculate radiance using the Gamma (Γ) and Riemann Zeta (ζ) functions as in ([Planck Collaboration et al. 2014](#)):

$$\mathcal{R} = \tau_{353} \frac{\sigma_S}{\pi} T^4 \left(\frac{kT}{h\nu_0} \right)^\beta \frac{\Gamma(4+\beta)\zeta(4+\beta)}{\Gamma(4)\zeta(4)}, \quad (1)$$

where σ_S is the Stefan-Boltzmann constant, h is the Planck constant, k is the Boltzmann constant and $\nu_0 = 3.53 \times 10^{11}$ Hz.

Fig. 1 shows the radiance for *premise*, GNILC and 2013 within two low signal to noise regions. Region one spans $(l, b) = (80-90^\circ, 70-80^\circ)$, region two spans $(l, b) = (-80-70^\circ, 270-280^\circ)$. The GNILC radiance maps visibly display a higher degree of smoothing and so fewer spatial features than the 2013 and *premise* radiance maps. To try and determine whether the additional features seen within the *premise* and 2013 radiance maps are entirely due to residual CIBA or are, in fact, thermal dust features which GNILC has smoothed out, we enlist the use of the HI4PI H_I column density maps. At high latitudes H_I column density traces thermal dust structure without being effected by CIBA.

We smooth the radiance maps to 16.2 arcmin and reduce their N_{side} to 1024 to enable a comparison with the column density data. Figs. 2 and 3 show the three radiance maps alongside the HI4PI map for both regions. Contours have been overlaid to highlight the pertinent features in each map, eight contour levels

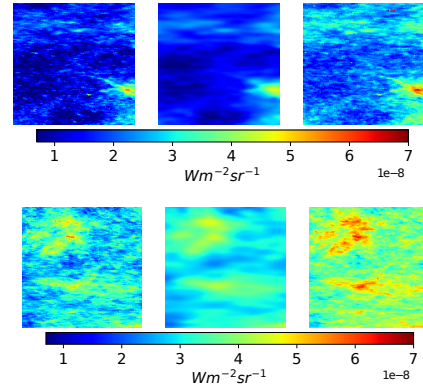


Fig. 1. Radiance maps for *premise*, GNILC and 2013 (from left to right) within $(l, b) = (80-90^\circ, 70-80^\circ)$ (top row) and $(l, b) = (-80-70^\circ, 270-280^\circ)$ (bottom row).

were chosen and smoothed over 32 pixels. Features can be seen within HI4PI column density maps which are most notably absent within the GNILC radiance maps: for region one the high intensity region within the lower left corner is least characterised by the GNILC radiance map, as is the lower left circular contour within region two.

In Fig. 4 we perform the same linear regression against $E(B-V)$ as in Fig. ?? but for the radiance estimates. Table 1 and 2 give the linear fit parameters. Again we see strong correlations between all three radiance estimates and both the SDSS and Green reddening values. **Am a bit confused as to why I can't get similar results to PR2 with the plot of radiance against SDSS E(B-V),**

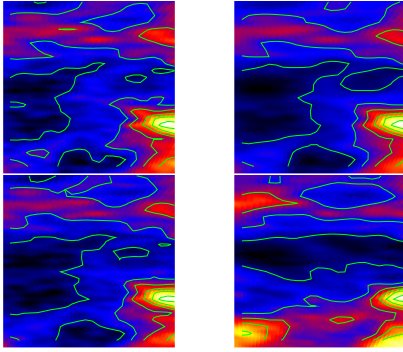


Fig. 2. Radiance maps alongside the HI4PI map within $(l, b) = (80\text{--}90^\circ, 70\text{--}80^\circ)$. (Clockwise from top left to bottom left:) premise radiance, GNILC radiance, HI4PI column density and 2013 radiance.

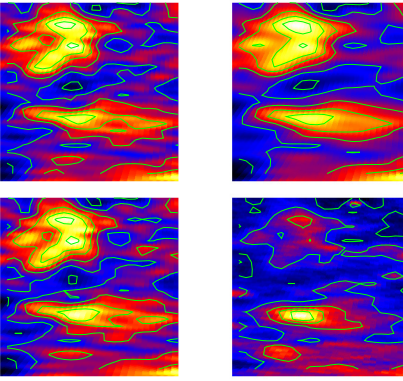


Fig. 3. Radiance maps alongside the HI4PI map within $(l, b) = (-80\text{--}70^\circ, 270\text{--}280^\circ)$. (Clockwise from top left to bottom left:) premise radiance, GNILC radiance, HI4PI column density and 2013 radiance.

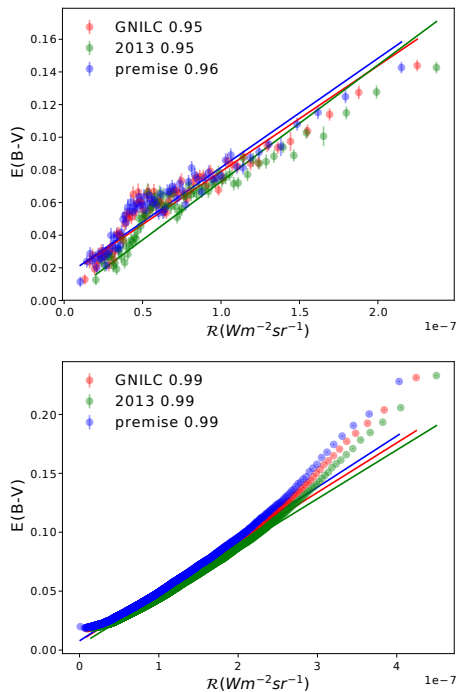


Fig. 4. Linear relationship between $E(B-V)$ and radiance for premise, GNILC and 2013. $E(B-V)$ values have been calculated using the SDSS quasars (top)/Green reddening map (bottom).

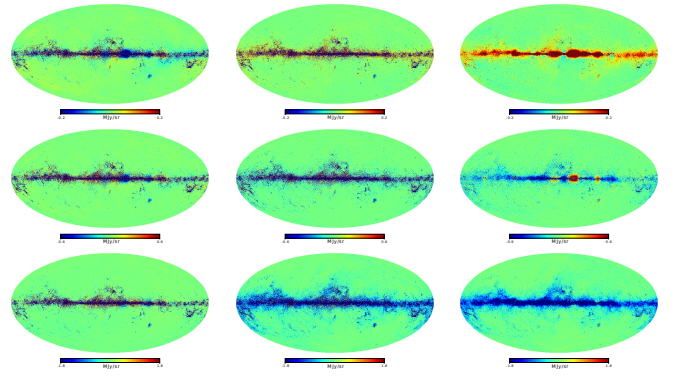


Fig. 5. Difference maps between the two thermal dust estimates at each frequency: 353, 545 and 857 GHz (top to bottom). (Left:) premise_{MBB} - GNILC_{MBB}, (middle:) premise_{MBB} - 2013_{MBB}, (right:) 2013_{MBB} - GNILC_{MBB}.

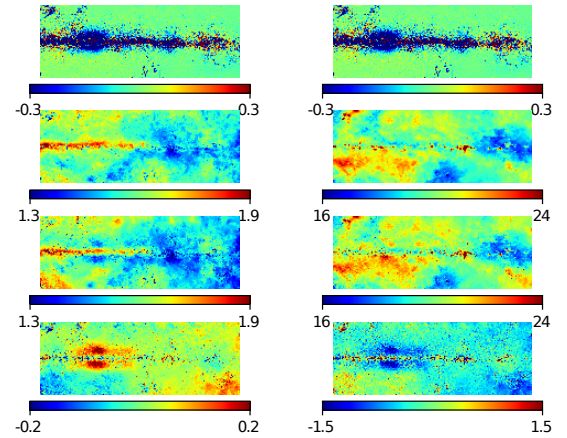


Fig. 6. Left: Cartesian projection of the central Galactic plane region of the Top: 353 GHz difference map, upper middle: premise spectral index map, lower middle: GNILC spectral index map, bottom: (premise - GNILC) spectral index map. Right: Same as on the left but for temperature.

Table 1. Linear regression parameters: SDSS reddening vs. radiance

Method	Gradient	Intercept
2013	$(7.14 \pm 0.28)10^5$	$(1.4 \pm 6.8)10^{-3}$
premise	$(6.68 \pm 0.26)10^5$	$(14.6 \pm 0.03)10^{-3}$
GNILC	$(6.48 \pm 0.23)10^5$	$(14.1 \pm 1.1)10^{-3}$

Table 2. Linear regression parameters: Green reddening map vs. radiance

Method	Gradient	Intercept
2013	$(4.14 \pm 0.01)10^5$	$(4.2 \pm 0.11)10^{-3}$
premise	$(4.35 \pm 0.01)10^5$	$(7.9 \pm 0.11)10^{-3}$
GNILC	$(4.21 \pm 0.01)10^5$	$(7.5 \pm 0.11)10^{-3}$

the pr2 gradient value is $(5.40 \pm 0.09) \times 10^{**4}$ and the error on the gradient is lower than when tau is used. I see a lower fractional gradient error for the Green reddening value and gradient values closer to the expected 5.40 BUT not for the SDSS reddening values. The SDSS regression is noisier for my radiance values than for my tau values which should not be the case.

Table 3. The various thermal dust estimates and the techniques used to form them.

Name	Technique
premise _{MBB}	$\tau_{353} \times B(T, \nu) \times \left(\frac{\nu}{353}\right)^{\beta} \times 10^{20} \times cc^{-1}$ (MJy/sr)
premise _{filt}	Filtered total flux maps
GNILC _{MBB}	$\tau_{353} \times B(T, \nu) \times \left(\frac{\nu}{353}\right)^{\beta} \times 10^{20} \times cc^{-1}$ (MJy/sr)
GNILC _{filt}	Filtered total flux maps
2013 _{MBB}	$\tau_{353} \times B(T, \nu) \times \left(\frac{\nu}{353}\right)^{\beta} \times 10^{20} \times cc^{-1}$ (MJy/sr)

0.2. Thermal dust maps

In this section we compare the premise thermal dust estimates to those produced by GNILC and 2013. 2013 have one set of thermal dust maps: those produced by reconstructing the MBB parameters. GNILC and premise, however first filter the total flux measurements and then fit the MBB model giving them both two thermal dust estimates: the filtered total flux maps and the reconstruction of their MBB parameters. Table 3 outlines our terminology for the various dust maps under investigation.

Note: we need to multiply the MBB models by 10^{20} for the conversion to MJy/sr and divide them by their own colour corrections (formed using each method's temperature and spectral index estimates). We have to re-apply the effects of the passbands in order to form CIB plus instrumental noise maps by subtracting these MBB models from the total flux maps which have not been colour corrected.

0.2.1. Thermal dust: reconstructed MBB parameters

Fig. 5 shows the difference between the premise_{MBB} and GNILC_{MBB}/2013_{MBB} thermal dust estimates at each frequency; as the Galactic plane has the highest thermal dust signal this region dominates these maps. At 353 GHz globules of negative differences can be seen in the premise_{MBB}/GNILC_{MBB} and 2013_{MBB}/GNILC_{MBB} difference maps along the Galactic plane, this is also the case at 545 GHz and again but too a lesser degree at 857 GHz. The most prominent 'globule' at all frequencies is situated just to the right of the Galactic centre. Fig. 6 show this particular region in detail within the 353 GHz difference map, the GNILC temperature and spectral index maps, the premise temperature and spectral index maps and the temperature and spectral index difference maps. The globular feature is also present in the temperature and spectral index difference maps and is caused by GNILC discerning temperature and spectral index features around the Galactic plane that are not seen by premise. Within and around the Galactic plane resolution is not an issue as both the premise and GNILC results are presented at 5 arcmin here. It is possible that these globular features along the Galactic plane relate to actual changes in the dust MBB temperature and spectral index but as neither premise nor 2013 see such features they could also be a feature of the GNILC processing.

Fig. 7 shows percentage difference maps at each frequency: the absolute difference between the premise_{MBB} and GNILC_{MBB}/2013_{MBB} dust estimates divided by the GNILC_{MBB}/2013_{MBB} dust map at each frequency. For all frequencies the largest differences are at high latitudes where the dust signal-to-noise is weakest and where the GNILC algorithm applies the greatest degree of smoothing. Along $b = 0^\circ$ the premise_{MBB} thermal dust estimate differs from the 2013_{MBB} and GNILC_{MBB} to a larger extent than the 2013_{MBB} and GNILC_{MBB} models differ. This highlights the difficulties the premise algorithm has in re-

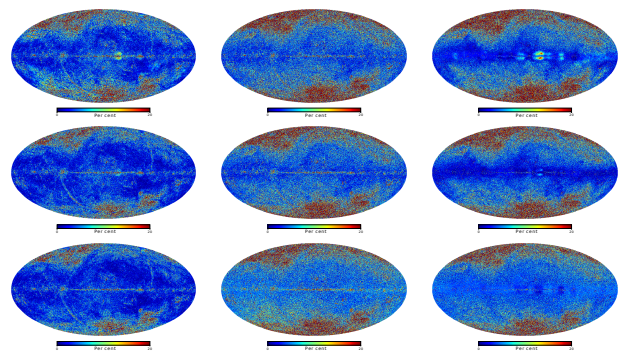


Fig. 7. Percentage difference maps between the MBB thermal dust estimates at each frequency: 353, 545 and 857 GHz (top to bottom). (Left:) premise_{MBB} - GNILC_{MBB}, (middle:) premise_{MBB} - 2013_{MBB}, (right:) 2013_{MBB} - GNILC_{MBB}.

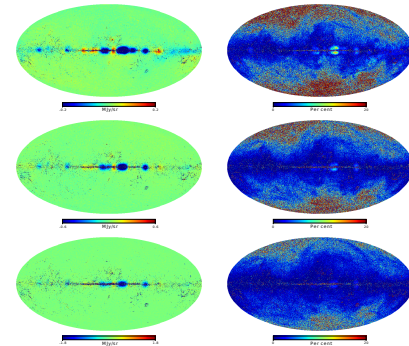


Fig. 8. Difference (left) and percentage(right) difference maps for premise_{filt} and GNILC_{filt} at each frequency: 353, 545 and 857 GHz (top to bottom).

covery model parameters across heavily masked regions. The GNILC globules are again visible across the Galactic plane at 353 GHz for both the premise_{MBB} and 2013_{MBB} percentage difference maps.

0.2.2. Thermal dust: filtered maps

Only premise and GNILC produce filtered dust estimates so the 2013 methodology is no longer considered in this section. Fig. 8 shows the differences and percentage differences between the premise_{filt} and GNILC_{filt} thermal dust estimates at each frequency. The GNILC globules are seen again indicating that if these feature are not real then they are a product of the GNILC filtering process, as opposed to the MBB fit. The highest percentage differences between premise_{filt} and GNILC_{filt} occur at $b = 0^\circ$ and the low dust signal-to-noise regions as with the GNILC_{MBB}/premise_{MBB} percentage difference map. The IRAS streaks are no longer visible as the 3000 GHz map is not given any additional weighting over the other frequencies within the premise filtering.

References

Planck Collaboration, Abergel, A., Ade, P. A. R., et al. 2014, A&A, 571, A11